

Pole determination of $X(3960)$ and $X_0(4140)$ in the decay $B^+ \rightarrow D_s^+ D_s^- K^+{}^*$

Jialiang Lu (卢家亮) Mao Song (宋昂)^{ID} Gang Li (李刚) Xuan Luo (罗旋)^{†ID}

Anhui University, Hefei 230601, China

Abstract: Two near-threshold peaking structures with spin-parities of $J^{PC} = 0^{++}$ were recently discovered by the LHCb Collaboration in the $D_s^+ D_s^-$ invariant mass distribution of the decay process $B^+ \rightarrow D_s^+ D_s^- K^+$. In our study, we employed a coupled-channel model to fit the experimental results published by the LHCb Collaboration, simultaneously fitting the model to the invariant mass distributions of $M_{D_s^+ D_s^-}$, $M_{D_s^+ K^+}$, and $M_{D_s^- K^+}$. We utilized a coupled-channel model to search for the poles of $X(3960)$ and $X_0(4140)$. The determination of the poles is meaningful in itself, and it also lays a foundation for future research on $X(3960)$ and $X_0(4140)$. Upon turning off the coupled-channel and performing another fit, we observed a change in the fitting quality, and the effect was almost entirely due to the peak of $X(3960)$. Therefore, we suggest that $X(3960)$ may not be a kinematic effect.

Keywords: hadron-hadron interactions, heavy-particle decays, quark model, strong interaction, exotic mesons, heavy mesons

DOI: 10.1088/1674-1137/ad9898 **CSTR:** 32044.14.ChinesePhysicsC.49023103

I. INTRODUCTION

For a long time, we have been asking the question, "What type of matter can be formed by quark models?" The traditional quark model successfully explains that baryons are complexes of three quarks and mesons are combinations of quarks and antiquarks. With the advancements in experimental methods, the recent discovery of candidates for the pentaquark and tetraquark states in experiments has expanded the scope of our study of traditional hadrons, which include qualitatively different $qqq\bar{q}\bar{q}$ and $qq\bar{q}\bar{q}$. In addition, more exotic structures have been observed in experiments; see Refs. [1–8]. To answer the appeal question, we must determine whether the pentaquark and tetraquark states exist.

In determining the strange state of quantum chromodynamics (QCD), the decay process of B mesons will be an important and effective platform. In this process, many candidates for strange hadron states can be observed. Over the past few years, major laboratories have successively discovered candidates for strange hadron states in the decay of B mesons, such as $Z_{cs}(4000)$ and $Z_{cs}(4000)$ [9], $X(4140)$ [10, 11] in $B^+ \rightarrow J/\psi \phi K^+$, and $X_0(2900)$ and $X_1(2900)$ in $B^+ \rightarrow D^+ D^- K^+$ decay [12, 13]. Referring to these experiments, we can observe that the three-body de-

cay of B mesons can provide much information on hadron resonance; see Refs. [14–17].

Very recently, the LHCb Collaboration reported a new near-threshold structure named $X(3960)$ in the $D_s^+ D_s^-$ invariant mass distribution of the decay $B^+ \rightarrow D_s^+ D_s^- K^+$. The peak structure is very close to the $D_s^+ D_s^-$ threshold with a statistical significance larger than 12σ . The mass, width, and quantum numbers of this structure were measured to be $M = 3956 \pm 5 \pm 10$ MeV, $\Gamma = 43 \pm 13 \pm 8$ MeV, and $J^{PC} = 0^{++}$. The LHCb analysis indicates that this structure is an exotic candidate consisting of $cs\bar{c}\bar{s}$ constituents. In addition, when checking the data of the $D_s^+ D_s^-$ invariant mass distribution, a dip is observed at approximately 4.14 GeV; the LHCb interpreted it as another structure named $X_0(4140)$ with a mass of $M = 4133 \pm 6 \pm 6$ MeV, width of $\Gamma = 67 \pm 17 \pm 7$ MeV, and quantum numbers of $J^{PC} = 0^{++}$ [18]. As analyzed by the LHCb Collaboration, $X_0(4140)$ might be caused by either a new resonance with the 0^{++} assignment or a $D_s^+ D_s^- J/\psi \phi$ coupled-channel effect, but no firm conclusion has been reached [18].

Many theoretical studies have shown much interest in X resonances. In recent years, many studies have used different models and technical methods to analyze the characteristics of exotic mesons $cs\bar{c}\bar{s}$ [19–26]. To deter-

Received 15 August 2024; Accepted 29 November 2024; Published online 30 November 2024

* Supported partly by the National Natural Science Foundation of China (12205002), the Natural Science Foundation of Anhui Province, China (2108085MA20, 2208085MA10), and the key Research Foundation of Education Ministry of Anhui Province of China (KJ2021A0061)

† E-mail: xuanluo@ahu.edu.cn

 Content from this work may be used under the terms of the Creative Commons Attribution 3.0 licence. Any further distribution of this work must maintain attribution to the author(s) and the title of the work, journal citation and DOI. Article funded by SCOAP³ and published under licence by Chinese Physical Society and the Institute of High Energy Physics of the Chinese Academy of Sciences and the Institute of Modern Physics of the Chinese Academy of Sciences and IOP Publishing Ltd

ine the origin and structure of $X(3960)$ in decay $B^+ \rightarrow D_s^+ D_s^- K^+$, scholars have proposed many explanations for the possibility of this structure. Because its mass is close to the $D_s^+ D_s^-$ threshold, this structure can be interpreted as a possible hadronic molecule. Refs. [27, 28] proposed to treat $X(3960)$ as the molecular state of $D_s^+ D_s^-$ with $J^{PC} = 0^{++}$ in the QCD sum rules approach. Another calculation with QCD two-point sum rules [29] results in the assignment that $X(3960)$ is a scalar diquark-antidiquark state. The calculations in the one-boson-exchange model [30] also favor the molecule interpretation. It can also be analyzed through the characteristics of $X(3960)$ using the coupled-channel method. The authors of Ref. [31] performed a coupled-channel calculation of the interaction $D\bar{D} - D_s^+ D_s^-$ in the chiral unitary approach and interpreted $X(3960)$ as a hadronic molecule in the coupled $D\bar{D} - D_s^+ D_s^-$ system [31–33]. The author of Ref. [34] interpreted $X(3960)$ as a $c\bar{s}\bar{c}\bar{s}$ state, whereas in Ref. [35], $X(3960)$ was interpreted as 0^{++} $c\bar{s}\bar{c}\bar{s}$ tetraquark states using an improved chromomagnetic interaction model. In addition, another study suggested that $X(3960)$ probably has the mixed characteristics of a $c\bar{c}$ confining state and $D_s\bar{D}_s$ continuum [36]. Some theoretical and experimental research has been conducted on $X_0(4140)$, but its origins are still debated. For instance, in Ref. [35], $X_0(4140)$ was also interpreted as $c\bar{s}\bar{c}\bar{s}$ tetraquark states. The discussion about mass and width in Ref. [29] enabled us to consider that the model is also acceptable. Because different computational models suggest different explanations, forming with new concepts and insights into this state can aid us in further understanding the origin of $X_0(4140)$.

In this study, we analyzed the decay process $B^+ \rightarrow D_s^+ D_s^- K^+$ as published by the LHCb Collaboration. We simulated a coupled-channel model to analyze the data [37] using the default model and fitting the $M_{D_s^+ D_s^-}$, $M_{D_s^+ K^+}$, and $M_{D_s^- K^+}$ of these three different invariant mass distributions. Using the amplitude provided by the coupled channel model, we address the following problems: (i) the pole position of $X(3960)$ and $X_0(4140)$ and (ii) whether the production of $X(3960)$ is solely due to a kinematic effect.

II. FRAMEWORK

The LHCb data reveal visible $X(3960)$ and $X_0(4140)$ structures around the $D_s\bar{D}_s$ and $D_s^*\bar{D}_s^*$ thresholds, respectively. Thus, we can reasonably assume that the structures are caused by the threshold cusps that are further enhanced or suppressed by hadronic rescatterings and the associated poles [37, 38]; see Fig. 1(a). Meanwhile, for the two peaks at 4260 and 4660 MeV, we refer to the suggestions given by the LHCb Collaboration and add two Breit-Weigner effects, as shown in Fig. 1(c). We assume that other possible mechanisms are absorbed by the direct decay mechanism in Fig. 1(b).

First, we present the amplitude for Fig. 1(a). The first vertex v_1 is a weak interaction, and the initial weak $B^+ \rightarrow D_s\bar{D}_s K^+$ vertex is

$$v_1 = c_{\alpha, B^+ K^+} f_{D_s\bar{D}_s}^0 F_{K^+ B^+}^0. \quad (1)$$

For the vertex of process $B^+ \rightarrow D_s^*\bar{D}_s^* K^+$, there are two cases of parity conservation and parity violation. For the former, the vertex of $B^+(0^-) \rightarrow D_s^*\bar{D}_s^*(0^+) K^+(0^-)$ is

$$v_1^{\text{pc}} = c_{D_s^*\bar{D}_s^*, B^+ K^+} \vec{\epsilon}_{D_s^*} \cdot \vec{\epsilon}_{\bar{D}_s^*} f_{D_s^*\bar{D}_s^*}^0 F_{K^+ B^+}^0, \quad (2)$$

in the latter case, the vertex of $B^+(0^-) \rightarrow D_s^*\bar{D}_s^*(1^+) K^+(0^-)$ is

$$v_1^{\text{pv}} = c_{D_s^*\bar{D}_s^*, B^+ K^+} \vec{p}_{K^+} \cdot (\vec{\epsilon}_{D_s^*} \times \vec{\epsilon}_{\bar{D}_s^*}) f_{D_s^*\bar{D}_s^*}^0 F_{K^+ B^+}^0. \quad (3)$$

The energy, momentum, and polarization vector of a particle x are denoted by E_x , p_x , and ϵ_x , respectively, and particle masses are obtained from Ref. [39]. $c_{\alpha, B^+ K^+}$ is a complex coupling constant, which represents $c_{D_s\bar{D}_s, B^+ K^+}$ and $c_{D_s^*\bar{D}_s^*, B^+ K^+}$. We introduce the form factors f_{ij}^L and F_{kl}^L , defined by

$$f_{ij}^L = \frac{1}{\sqrt{E_i E_j}} \left(\frac{\Lambda^2}{\Lambda^2 + q_{ij}^2} \right)^{2+\frac{L}{2}}, \quad (4)$$

$$F_{kl}^L = \frac{1}{\sqrt{E_k E_l}} \left(\frac{\Lambda^2}{\Lambda^2 + \tilde{p}_k^2} \right)^{2+\frac{L}{2}}, \quad (5)$$

where q_{ij} is the momentum of i in the ij center-of-mass frame, and \tilde{p}_k is the momentum of k in the total center-of-mass frame. Λ is a cutoff, and $\Lambda = 1$ GeV. We use a common value of the cutoff for all the interaction vertices.

The second vertex v_2 is hadron scattering; the perturbative interactions for $D_s\bar{D}_s(D_s^*\bar{D}_s^*) \rightarrow D_s\bar{D}_s$ are given by s -wave separable interactions. For $D_s\bar{D}_s(0^+) \rightarrow D_s^+ D_s^-(0^+)$,

$$v_2 = h_{D_s^+ D_s^-, D_s\bar{D}_s} f_{D_s^+ D_s^-}^0 f_{D_s\bar{D}_s}^0, \quad (6)$$

and for $D_s^*\bar{D}_s^*(0^+) \rightarrow D_s^+ D_s^-(0^+)$,

$$v_2 = h_{D_s^+ D_s^-, D_s^*\bar{D}_s^*} \vec{\epsilon}_{D_s^*} \cdot \vec{\epsilon}_{\bar{D}_s^*} f_{D_s^+ D_s^-}^0 f_{D_s^*\bar{D}_s^*}^0. \quad (7)$$

Another vertex exists between the two vertices, which is the coupling of the two loops, which we denote as v_3 . The coupling of different loops is similar in form; for

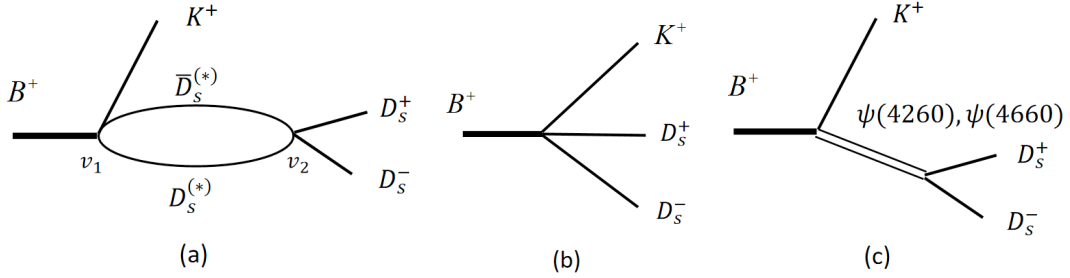


Fig. 1. Contributions of three mechanisms in the decay $B^+ \rightarrow D_s^+ D_s^- K^+$. (a) Coupled-channel; (b) Direct production; (c) Breit-Weigner effects.

$$D_s(0^-)\bar{D}_s(0^-) \rightarrow D_s(0^-)\bar{D}_s(0^-),$$

$$A_{\text{dir}} = c_{D_s\bar{D}_s, B^+ K^+} f_{D_s^+ D_s^-}^0 F_{K^+ B^+}. \quad (15)$$

$$v_3 = G_{D_s\bar{D}_s, D_s\bar{D}_s}(M_{D_s^+ D_s^-}), \quad (8)$$

for $D_s(0^-)\bar{D}_s(0^-) \rightarrow D_s^*(1^-)\bar{D}_s^*(1^-)$,

$$v_3 = \vec{\epsilon}_{D_s^*} \cdot \vec{\epsilon}_{\bar{D}_s^*} G_{D_s^*\bar{D}_s^*, D_s\bar{D}_s}(M_{D_s^+ D_s^-}), \quad (9)$$

for $D_s^*(1^-)\bar{D}_s^*(1^-) \rightarrow D_s(0^-)\bar{D}_s(0^-)$,

$$v_3 = \vec{\epsilon}_{D_s^*} \cdot \vec{\epsilon}_{\bar{D}_s^*} G_{D_s\bar{D}_s, D_s^*\bar{D}_s^*}(M_{D_s^+ D_s^-}), \quad (10)$$

and for $D_s^*(1^-)\bar{D}_s^*(1^-) \rightarrow D_s^*(1^-)\bar{D}_s^*(1^-)$,

$$\begin{aligned} v_3 &= \vec{\epsilon}_{D_s^*} \cdot \vec{\epsilon}_{\bar{D}_s^*} \vec{\epsilon}_{D_s^*} \cdot \vec{\epsilon}_{\bar{D}_s^*} G_{D_s^*\bar{D}_s^*, D_s^*\bar{D}_s^*}(M_{D_s^+ D_s^-}) \\ &= 3G_{D_s^*\bar{D}_s^*, D_s^*\bar{D}_s^*}(M_{D_s^+ D_s^-}). \end{aligned} \quad (11)$$

We introduce $[G^{-1}]_{\beta\alpha}(E) = [\delta_{\beta\alpha} - h_{\beta,\alpha}\sigma_\alpha(E)]$, where $h_{\beta,\alpha}$ is a coupling constant, and α and β are label interaction channels, with

$$\sigma_{D_s\bar{D}_s}(E) = \int dq q^2 \frac{[f_{D_s\bar{D}_s}^0(q)]^2}{E - E_{D_s}(q) - E_{\bar{D}_s}(q) + i\epsilon}, \quad (12)$$

$$\sigma_{D_s^*\bar{D}_s^*}(E) = \int dq q^2 \frac{[f_{D_s^*\bar{D}_s^*}^0(q)]^2}{E - E_{D_s^*}(q) - E_{\bar{D}_s^*}(q) + i\epsilon}. \quad (13)$$

With the above ingredients, the amplitudes for the Fig. 1(a) are respectively given by

$$\begin{aligned} A &= 4\pi f_{D_s^+ D_s^-}^0(p_{D_s^+}) F_{K^+ B^+}^0 \sum_{\alpha} \sum_{\beta} \\ &\times c_{\alpha, B^+ K^+} G_{\beta\alpha}(M_{D_s^+ D_s^-}) h_{D_s^+ D_s^- \beta} \sigma_{\beta}. \end{aligned} \quad (14)$$

Regarding the direct decay mechanism of Fig. 1(b),

Finally, we consider the Breit-Weigner mechanism of Fig. 1(c):

$$A_{\psi(4260)}^{1^-} = c_{\psi(4260)} \frac{\vec{p}_{K^+} \cdot \vec{p}_{D_s^+} f_{D_s^+ D_s^- \psi}^1 f_{\psi K^+, B^+}^1}{E - E_{K^+} - E_{\psi} + \frac{i}{2}\Gamma_{\psi(4260)}}, \quad (16)$$

$$A_{\psi(4660)}^{1^-} = c_{\psi(4660)} \frac{\vec{p}_{K^+} \cdot \vec{p}_{D_s^+} f_{D_s^+ D_s^- \psi}^1 f_{\psi K^+, B^+}^1}{E - E_{K^+} - E_{\psi} + \frac{i}{2}\Gamma_{\psi(4660)}}, \quad (17)$$

where \vec{p}_{K^+} is the B^+ CM, and $\vec{p}_{D_s^+}$ is the $D_s^+ D_s^-$ CM; the form factor defined by

$$f_{D_s^+ D_s^- \psi}^1 = \frac{1}{\sqrt{E_{D_s^+} E_{D_s^-} m_{\psi}}} \left(\frac{\Lambda^2}{\Lambda^2 + q_{D_s^+ D_s^-}^2} \right)^{\frac{5}{2}}, \quad (18)$$

$$f_{\psi K^+, B^+}^1 = \frac{1}{\sqrt{E_{\psi} E_{K^+} E}} \left(\frac{\Lambda^2}{\Lambda^2 + q_{\psi K^+}^2} \right)^{\frac{5}{2}}, \quad (19)$$

with constants $c_{\psi(4260)}$ and $c_{\psi(4660)}$.

III. RESULTS

We simultaneously fit the invariant mass distributions of $M_{D_s^+ D_s^-}$, $M_{D_s^+ K^+}$, and $M_{D_s^- K^+}$ from the LHCb Collaboration using the amplitudes of Eq. (14). The amplitude includes the vertices of the weak interaction and the adjustable coupling constant resulting from the hadron interaction; this includes $c_{D_s\bar{D}_s, B^+ K^+}$, $c_{D_s^*\bar{D}_s^*, B^+ K^+}$, $c_{\psi(4260)}$, $c_{\psi(4660)}$, $h_{D_s\bar{D}_s, D_s\bar{D}_s}$, $h_{D_s^*\bar{D}_s^*, D_s\bar{D}_s}$, $h_{D_s^*\bar{D}_s^*, D_s\bar{D}_s}$, and $h_{D_s^*\bar{D}_s^*, D_s\bar{D}_s}$. To reduce the number of fitting parameters, we set $h_{D_s\bar{D}_s, D_s\bar{D}_s} = h_{D_s^*\bar{D}_s^*, D_s\bar{D}_s}$, as making them different does not significantly affect the quality of the fit. Because the coupling and interaction constants of hadron scattering are consistent, we can further reduce the fitting parameters.

ers. Finally, because the magnitude and phase of the full amplitude are arbitrary, our default model has a total of nine fitting parameters. Our default model has a total of 8 (7+1) fitting parameters, in addition to these seven parameters as constants, the last parameter added is the overall factor. The parameters obtained from the final fit are shown in Table 1.

We show the default model by the solid blue curves in Fig. 2, which closely matches the LHCb data. We can clearly observe the peak at 3960 MeV and a dip at 4140 MeV. The fitting quality is $\chi^2/\text{ndf} = (55.67 + 44.66 + 56.08)/(127 - 8) \approx 1.31$, where three χ^2 values result from three different distributions; "ndf" is the number of bins (43 for $D_s^+ D_s^-$, 42 for $D_s^+ K^+$, and 42 for $D_s^- K^+$) subtracted by the number of fitting parameters.

We also show the different contributions of the chart in Fig. 2. The solid orange curves represent the contribution of $D_s^+ D_s^-$ single channel, and the dotted green curves represent the contribution of $D_s^* \bar{D}_s^*$ single channel. Generally, the solid orange curves play a dominant role throughout the entire process, particularly in relation to

the peak of $X(3960)$. This behavior can be attributed to the fact that the $X(3960)$ peak primarily results from the threshold of $D_s^+ D_s^-$. For the peaks at 4260 and 4660 MeV, we adopted the same method as the LHCb Collaboration and introduced two Breit-Wigner effects [40, 41], $\psi(4260)$ and $\psi(4660)$, which are represented by purple and brown dotted curves, respectively. The analysis here is generally consistent with the analysis given by LHCb; for two peaks near 4260 and 4660 MeV, the final fitting results have been significantly improved.

In our study, we conducted a search for poles in the default $D_s \bar{D}_s D_s^* \bar{D}_s^*$ coupled-channel scattering amplitude using analytic continuation. We observed the poles of $X(3960)$ and $X_0(4140)$, which are summarized in Table 2. Additionally, in the table, we also list the Riemann sheets of the poles by $(D_s \bar{D}_s D_s^* \bar{D}_s^*)$, where $s_\alpha = p$ indicates that the pole is located on the physical p sheet of the channel, whereas $s_\alpha = u$ indicates that it is on the unphysical u sheet of the channel. As shown in the table, we can obtain the positions of $X(3960)$ and $X_0(4140)$. Based on this, we can suggest that $X(3960)$ is a resonance state and

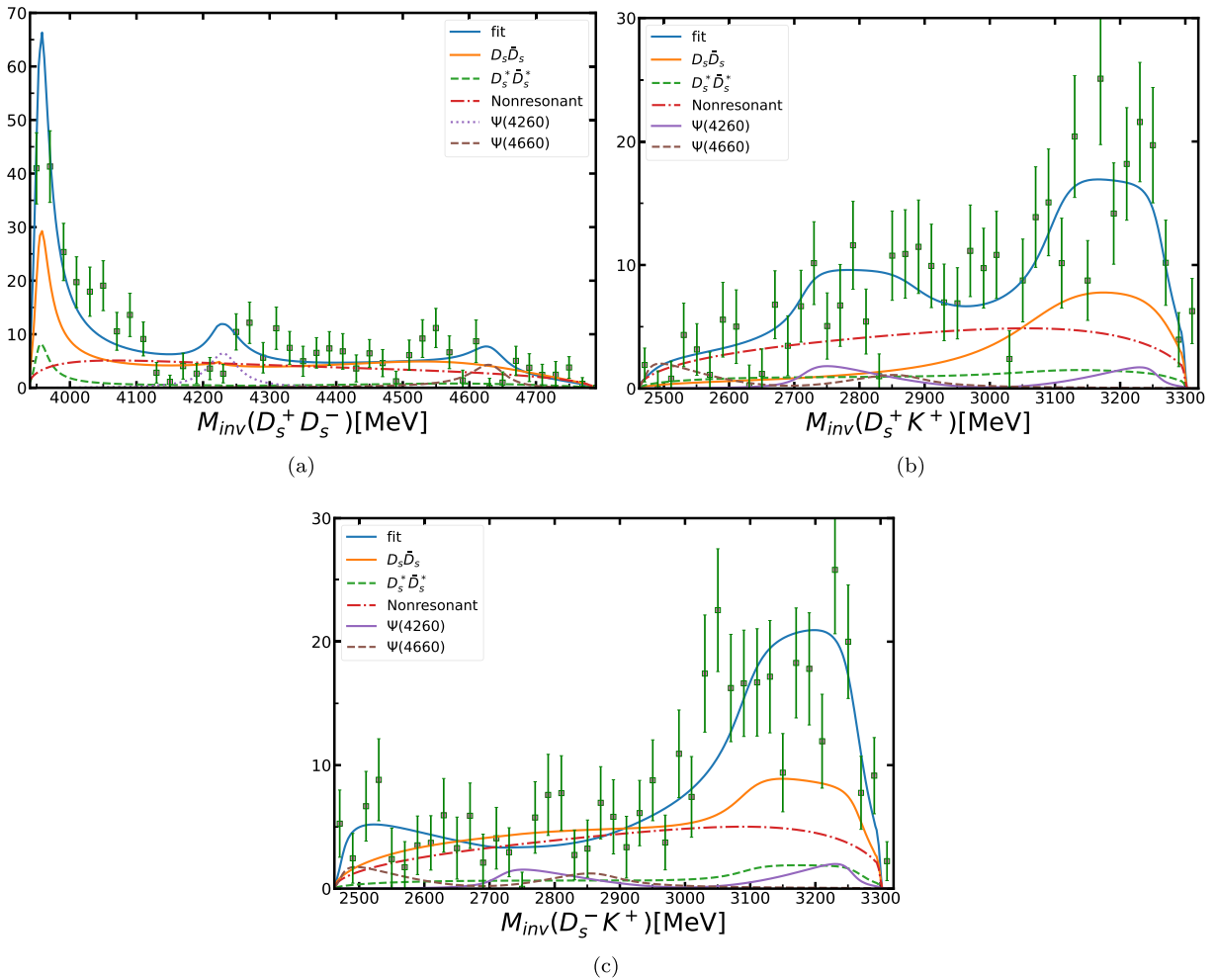


Fig. 2. (color online) (a) $D_s^+ D_s^-$, (b) $D_s^+ K^+$, (c) $D_s^- K^+$ invariant mass distributions for $B^+ \rightarrow D_s^+ D_s^- K^+$.

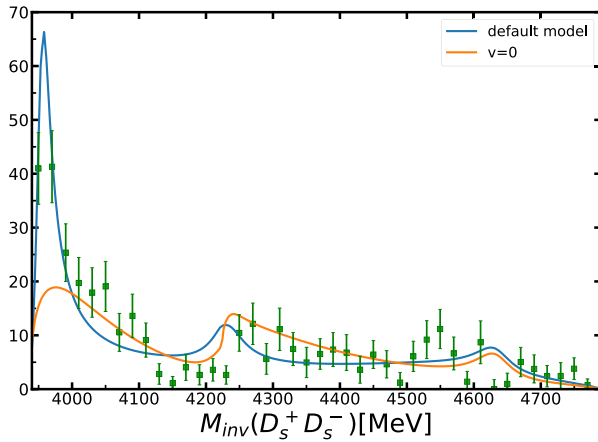


Fig. 3. (color online) Comparison of different models. The blue line in the figure is for the default model, whereas the orange line is for the model that turns off the couple-channel effect.

Table 1. Parameter values for $B^+ \rightarrow D_s^+ D_s^- K^+$ models. The second and third columns are for the default and no couple-channel effect models.

$c_{D_s \bar{D}_s, B^+ K^+}$	-0.07+0.23i	-0.39+0.45i
$c_{D_s^* \bar{D}_s^*, B^+ K^+}$	-0.13+0.09i	-0.01+0.58i
$c_{\psi(4260)}$	2.26–2.46i	8.21–0.77i
$c_{\psi(4660)}$	-3.27+5.30i	-8.98–13.08i
$h_{D_s \bar{D}_s, D_s \bar{D}_s}$	13.18+5.94i	3.83+16.02i
$h_{D_s^* \bar{D}_s^*, D_s^* \bar{D}_s^*}$	-17.10+18.21i	0
$h_{D_s^* \bar{D}_s^*, D_s \bar{D}_s}$	-15.14–11.10i	-1.47+10.20i
Λ/MeV	1000 (fixed)	1000 (fixed)

Table 2. $X(3960)$ and $X_0(4140)$ poles in the default model. Pole positions (in MeV) and their Riemann sheets (see the text for notation) are given in the second and third columns, respectively.

$X(3960)$	3952.48+12.46i	(pu)
$X_0(4140)$	4142.48	(pp)

$X_0(4140)$ is a virtual state [42, 43]. This observation is consistent with the results shown in Fig. 2, which clearly indicate that the formation of $X(3960)$ is primarily due to the interaction of $V_{D_s^+ D_s^-, D_s^+ D_s^-}$. Even without considering the contribution of $V_{D_s^+ D_s^-, D_s^* \bar{D}_s^*}$ and $V_{D_s^* \bar{D}_s^*, D_s^+ \bar{D}_s^-}$, the state of $X(3960)$ can be understood as a bound state of $D_s^+ D_s^-$. The behavior of the green dotted curves in Fig. 2(a) further supports the notion that if $X_0(4140)$ is a virtual state, the

contribution of $V_{D_s^* \bar{D}_s^*, D_s^* \bar{D}_s^*}$ is weak.

In order to investigate the threshold effect of the kinematic effect in the vicinity and determine whether the $X(3960)$ peak structure is solely caused by the $D_s \bar{D}_s$ threshold, we disabled the coupled-channel effect, equivalent to directly finding the monocyclic graph contribution of the Fig. 1. The data was then re-fitted, as shown in the Table 2. In Fig. 3, although the overall change in χ^2 is small, it is evident that the height of the first peak undergoes a significant change, and the change in χ^2 is primarily due to this peak. Therefore, we can conclude that the pure kinematic effect alone is insufficient to form a peak structure. The peak structure should indicate a state that actually exists.

IV. CONCLUSION

We analyze the observations of the LHCb Collaboration on the decay process $B^+ \rightarrow D_s^+ D_s^- K^+$. Note that when calculating the total amplitude, we refer to the work of the LHCb Collaboration and introduce the Breit-Weigner effect of the resonance state $\psi(4260)$, but the peak value of $\psi(4260)$ is slightly earlier than the jump position in the data of the invariant mass spectrum of $D_s^+ D_s^-$, and this position is very close to the threshold of $D \bar{D}$. Therefore, we can reasonably expect that building a new model based on our current model and adding $D \bar{D}$ this coupled-channel will be useful in explaining the jump in the invariant mass spectrum of $D_s^+ D_s^-$. Our default model fits the $M_{D_s^+ D_s^-}$, $M_{D_s^+ K^+}$, and $M_{D_s^- K^+}$ of these three different invariant mass distributions simultaneously, and the final fitting quality is $\chi^2/ndf \approx 1.31$.

Without adding resonance states directly, we search the poles of $X(3960)$ and $X_0(4140)$ using the coupled-channel model and finally determine the positions of $X(3960)$ and $X_0(4140)$. From this, we suggest that $X(3960)$ may be a resonance state and $X_0(4140)$ may be a virtual state. The determination of the pole positions is meaningful, which provides information for the research on $X(3960)$ and $X_0(4140)$ and lays a certain foundation for the study of their properties in the future. By turning off the coupled-channel effect and fitting the data again, we find that the overall fitting quality does not change significantly. However, the final fitting result shows that the influence is relatively large at the position of $X(3960)$, and almost all the changes of χ^2 result from the $X(3960)$ peak. Therefore, we suggest that the pure kinematic effect is insufficient to form the $X(3960)$ peak structure. This conclusion provides certain reference value for future research.

References

- [1] H.-X. Chen, W. Chen, X. Liu *et al.*, [Phys. Rept. 639, 1 \(2016\)](#), arXiv: 1601.02092[hep-ph]

- [2] A. Hosaka, T. Iijima, K. Miyabayashi *et al.*, [PTEP 062, 062C01 \(2016\)](#), arXiv: 1603.09229[hep-ph]

- [3] R. F. Lebed, R. E. Mitchell, and E. S. Swanson, *Prog. Part. Nucl. Phys.* **93**, 143 (2017), arXiv: 1610.04528[hepph]
- [4] A. Esposito, A. Pilloni, and A. D. Polosa, *Phys. Rept.* **668**, 1 (2017), arXiv: 1611.07920[hep-ph]
- [5] A. Ali, J. S. Lange, and S. Stone, *Prog. Part. Nucl. Phys.* **97**, 123 (2017), arXiv: 1706.00610[hep-ph]
- [6] F.-K. Guo, C. Hanhart, U.-G. Meißner *et al.*, *Rev. Mod. Phys.* **90**, 015004 (2018), arXiv: 1705.00141[hep-ph]
- [7] S. L. Olsen, T. Skwarnicki, and D. Zieminska, *Rev. Mod. Phys.* **90**, 015003 (2018), arXiv: 1708.04012[hep-ph]
- [8] N. Brambilla, S. Eidelman, C. Hanhart *et al.*, *Phys. Rept.* **873**, 1 (2020), arXiv: 1907.07583[hep-ex]
- [9] R. Aaij *et al.* (LHCb), *Phys. Rev. Lett.* **127**, 082001 (2021), arXiv: 2103.01803[hep-ex]
- [10] T. Aaltonen *et al.* (CDF), *Phys. Rev. Lett.* **102**, 242002 (2009), arXiv: 0903.2229[hep-ex]
- [11] V. M. Abazov *et al.* (D0), *Phys. Rev. D* **89**, 012004 (2014), arXiv: 1309.6580[hep-ex]
- [12] R. Aaij *et al.* (LHCb), *Phys. Rev. Lett.* **125**, 242001 (2020), arXiv: 2009.00025[hep-ex]
- [13] R. Aaij *et al.* (LHCb), *Phys. Rev. D* **102**, 112003 (2020), arXiv: 2009.00026[hep-ex]
- [14] Z. P. Xing, F. Huang, and W. Wang, *Phys. Rev. D* **106**, 114041 (2022), arXiv: 2203.13524[hep-ph]
- [15] M. Y. Duan, E. Wang, and D. Y. Chen, (2023), arXiv: 2305.09436[hep-ph]
- [16] W. T. Lyu, Y. H. Lyu, M. Y. Duan *et al.*, (2023), arXiv: 2306.16101[hep-ph]
- [17] X. Q. Li, L. J. Liu, E. Wang *et al.*, (2023), arXiv: 2307.04324[hep-ph]
- [18] R. Aaij *et al.* (LHCb), *Phys. Rev. Lett.* **131**, 071901 (2023), arXiv: 2210.15153[hep-ex]
- [19] J. Nieves and M. P. Valderrama, *Phys. Rev. D* **86**, 056004 (2012), arXiv: 1204.2790[hep-ph]
- [20] Z.-G. Wang, *Eur. Phys. J. C* **74**, 2874 (2014), arXiv: 1311.1046[hep-ph]
- [21] R. F. Lebed and A. D. Polosa, *Phys. Rev. D* **93**, 094024 (2016), arXiv: 1602.08421[hep-ph]
- [22] W. Chen, H. X. Chen, X. Liu *et al.*, *Phys. Rev. D* **96**, 114017 (2017), arXiv: 1706.09731[hep-ph]
- [23] L. Meng, B. Wang, and S.-L. Zhu, *Sci. Bull.* **66**, 1288 (2021), arXiv: 2012.09813[hep-ph]
- [24] S. S. Agaev, K. Azizi, and H. Sundu, *Phys. Rev. D* **95**, 114003 (2017), arXiv: 1703.10323[hep-ph]
- [25] H. Sundu, S. S. Agaev, and K. Azizi, *Phys. Rev. D* **98**, 054021 (2018), arXiv: 1805.04705[hep-ph]
- [26] S. S. Agaev, K. Azizi, and H. Sundu, *Phys. Rev. D* **106**, 014025 (2022), arXiv: 2203.02542[hep-ph]
- [27] H. Mutuk, *Eur. Phys. J. C* **82**, 1142 (2022), arXiv: 2211.14836[hep-ph]
- [28] Q. Xin, Z. G. Wang, and X. S. Yang, *AAPPS Bull.* **32**, 37 (2022), arXiv: 2207.09910[hep-ph]
- [29] S. S. Agaev, K. Azizi, and H. Sundu, *Phys. Rev. D* **107**, 054017 (2023), arXiv: 2211.14129[hep-ph]
- [30] R. Chen and Q. Huang, (2022), arXiv: 2209.05180[hepph]
- [31] M. Bayar, A. Feijoo, and E. Oset, *Phys. Rev. D* **107**, 034007 (2023), arXiv: 2207.08490[hep-ph]
- [32] T. Ji, X. K. Dong, M. Albaladejo *et al.*, *Phys. Rev. D* **106**, 094002 (2022), arXiv: 2207.08563[hep-ph]
- [33] T. Ji, X. K. Dong, M. Albaladejo *et al.*, *Sci. Bull.* **68**, 688 (2023), arXiv: 2212.00631[hep-ph]
- [34] A. M. Badalian and Y. A. Simonov, *Eur. Phys. J. C* **83**, 410 (2023), arXiv: 2301.13597[hep-ph]
- [35] T. Guo, J. Li, J. Zhao *et al.*, *Chin. Phys. C* **47**, 063107 (2023), arXiv: 2211.10834[hep-ph]
- [36] Y. Chen, H. Chen, C. Meng *et al.*, *Eur. Phys. J. C* **83**, 381 (2023), arXiv: 2302.06278[hepph]
- [37] S. X. Nakamura and J. J. Wu, *Phys. Rev. D* **108**, L011501 (2023), arXiv: 2208.11995[hep-ph]
- [38] X. K. Dong, F. K. Guo, and B. S. Zou, *Phys. Rev. Lett.* **126**, 152001 (2021), arXiv: 2011.14517[hep-ph]
- [39] P. A. Zyla *et al.* (Particle Data Group), *PTEP* **2020**, 083C01 (2020)
- [40] Q. F. Cao, H. R. Qi, G. Y. Tang *et al.*, *Eur. Phys. J. C* **81**, 83 (2021), arXiv: 2002.05641[hep-ph]
- [41] Q. F. Cao, H. R. Qi, Y. F. Wang *et al.*, *Phys. Rev. D* **100**, 054040 (2019), arXiv: 1906.00356[hepph]
- [42] N. Suzuki, T. Sato, and T. S. H. Lee, (2009), arXiv: 0910.1742[nucl-th]
- [43] N. Suzuki, T. Sato, and T. S. H. Lee, *Phys. Rev. C* **79**, 025205 (2009), arXiv: 0806.2043[nucl-th]